Quantitative insights into regime-dependent aerosol pH variability in ~~an~~ ammonia-rich urban Beijing~~atmosphere~~ from explainable machine learning

Jing Duan[1,†], Ting Wang[1,†], Ru-Jin Huang[1,2,3*], Jingye Ren[1], Haobin Zhong[4], Wei Xu[5], Chunshui Lin[1], Yanan Zhan[1,2], Huabin Huang[6], Yongjie Li[7]

[1]State Key Laboratory of Loess Science, Institute of Earth Environment, Chinese Academy of Sciences, Xi'an 710061, China

[2]Institute of Global Environmental Change, Xi'an Jiaotong University, Xi'an 710049, China

[3]University of Chinese Academy of Sciences, Beijing 100049, China

[4]School of Advanced Materials Engineering, Jiaxing Nanhu University, Jiaxing, 314001, China

[5]State Key Laboratory of Advanced Environmental Technology, Institute of Urban Environment, Chinese Academy of Sciences, Xiamen, China

[6]College of Environment and Public Health, Xiamen Huaxia University, Xiamen 361024, China

[7]Department of Civil and Environmental Engineering, Faculty of Science and Technology, University of Macau, Taipa, Macau SAR 999078, China

Correspondence to: Ru-Jin Huang (rujin.huang@ieecas.cn)

†Contributed equally to this study

Abstract

Aerosol acidity (pH) plays a crucial role in atmospheric chemistry. Meteorological conditions and chemical properties jointly contribute to pH variation, yet their behavior differs across environmental regimes and remains incompletely understood. Here, we integrate machine learning with interpretable model analyses, field observations, and thermodynamic modeling to quantitatively assess the relative contributions and associations of key factors to aerosol pH variability in the ammonia-rich urban atmosphere of Beijing. ~~in an ammonia-rich urban atmosphere.~~ Temperature exhibits a strong negative association with~~contribution to~~ pH variation, with an average decrease of ~0.6 units per 10 °C increase. Excess ammonia, nitrate-to-sulfate mass ratio (N/S), and PM_1 mass loading are positively associated with pH, showing stronger sensitivities at lower values and diminishing responses at higher levels. In contrast, the

contribution of relative humidity (RH) depends strongly on its interactions with temperature, aerosol composition, and mass loading, resulting in pronounced regime-dependent reversals. Higher RH is associated with enhanced aerosol acidity under low-temperature (< ~15 °C), nitrate-dominant (N/S > ~1.25), or high-mass (PM_1 > ~50 μg m^{-3}) conditions, whereas the opposite tendency occurs under warmer, sulfate-dominant, or low-mass regimes. This study provides new quantitative insights into the coupled meteorological and chemical modulation of pH and highlights the importance of multifactor interactions in understanding aerosol acidity variability in real-world atmospheres.

1. Introduction

Aerosol acidity (pH) critically modulates atmospheric multiphase processes, influencing gas–particle partitioning (Guo et al., 2016; Guo et al., 2017), secondary aerosol formation (Shi et al., 2019; Yang et al., 2022), pollutant transformation (Cao et al., 2020; Fu et al., 2022), and metal solubility (Tao and Murphy, 2019; Giorio et al., 2022), with important implications for air quality, climate, and human health (Mo et al., 2017; Myriokefalitakis et al., 2018; Su et al., 2020; Tilgner et al., 2021; Wei et al., 2023; Xie et al., 2023). Due to challenges in direct measurements, aerosol pH is commonly derived from thermodynamic equilibrium models such as ISORROPIA II and E-AIM, which estimate pH from observed chemical compositions and meteorological parameters (Clegg et al., 2001; Fountoukis and Nenes, 2007; Hennigan et al., 2015). Using such model-derived calculations, previous studies have reported globally variable aerosol acidity (Guo et al., 2016; Liu et al., 2017; Sharma et al., 2022). In China, aerosols generally exhibit higher pH relative to the United States and Europe, owing to its rich ammonia emission, and show distinct north–south gradients influenced by regional emissions and meteorology (Ding et al., 2019; Wang et al., 2020; Zhang et al., 2021).

Driving factors of aerosol pH in China's ammonia-rich environment have been explored in recent years using sensitivity analyses, yet a comprehensive understanding remains incomplete. For instance, Ding et al. (2019) identified sulfate, total ammonia, and temperature as common drivers of pH variations, with nitrate exerting less influence. In contrast, Xie et al. (2020) suggested that increases in the nitrate fraction, rather than ammonia, can elevate pH. Proposing a multiphase buffer theory, Zheng et al. (2020) showed that aerosol water content and particle

mass may outweigh chemical composition in controlling pH in ammonia-rich regions. Long-term observations, however, pointed to meteorology (temperature and relative humidity) as the dominant factors for seasonal and diurnal pH variability (Zhou et al., 2022; Duan et al., 2025). These discrepancies indicate that the coupled contributions of chemical and meteorological factors to aerosol pH variation are complex and strongly regime-dependent, warranting further comprehensive investigation. Importantly, decomposition of pH variation has primarily focused on the linear additive contributions of individual factors, relying on thermodynamic sensitivity tests and simple quantitative frameworks (Tao and Murphy, 2021; Wang et al., 2022; Zhou et al., 2022), while providing limited insight into potential nonlinear interactions among chemical and meteorological parameters that may jointly shape pH dynamics. Addressing this gap is therefore essential for achieving a more mechanistic understanding of aerosol acidity under different atmospheric environments.

Machine learning (ML) methods, combined with interpretable techniques such as Shapley Additive Explanations (SHAP), have emerged as powerful tools for capturing nonlinear relationships and high-dimensional dependencies in atmospheric studies (Grange et al., 2018; Hou et al., 2022; Song et al., 2022). SHAP provides a unified framework for quantifying the marginal contributions of individual predictors and their nonlinear interactions (Lundberg et al., 2020), making it particularly suitable for assessing how chemical composition and meteorological conditions jointly relate to atmospheric processes (Hou et al., 2022; Dai et al., 2023; Peng et al., 2023). In this study, we integrate thermodynamic model calculations with a SHAP-based ML framework to provide quantitative insights into the relative contributions of key factors to aerosol pH variability in an ammonia-rich atmosphere. Based on a full year of continuous observations from a northern Chinese city, this approach characterizes how chemical composition and meteorological conditions are jointly associated with aerosol acidity, quantifies their statistical interactions across diverse environmental regimes, and advances understanding of the processes underlying aerosol pH variation.

2. Materials and methods

2.1 Field observations

Continuous measurements were conducted from 21 December 2014 to 31 December 2015 at

an urban site located on the rooftop of the National Center for Nanoscience in Beijing (39.99°N, 116.32°E). Non-refractory PM_1 species, including organics (OA), sulfate (SO_4^{2-}), nitrate (NO_3^-), ammonium (NH_4^+), and chloride (Cl^-), were quantified using an Aerodyne quadrupole aerosol chemical speciation monitor (Q-ACSM) (Ng et al., 2011). Gaseous ammonia (NH_3) was measured with a Picarro G2103 analyzer (Maasikmets et al., 2015). Meteorological parameters, including temperature and relative humidity (RH), were simultaneously recorded using an automatic weather station (MAWS201, Vaisala, Finland) (Wang et al., 2017). Details on sampling and instrumentation are provided in Text S1.

2.2 Aerosol pH calculation

Aerosol pH was estimated using the ISORROPIA II thermodynamic model (Fountoukis and Nenes, 2007). The input dataset included the measured concentrations of SO_4^{2-}, NO_3^-, Cl^-, and total ammonia (NH_3+NH_4^+), together with meteorological parameters (RH and temperature). The model outputs, including hydronium ion concentration (H_{air}^+) and aerosol liquid water content (ALWC), were subsequently adopted to calculate PM_1 pH according to Eq (1) (Guo et al., 2015):

$$\mathrm{pH} = -\mathrm{Log}_{10}\gamma_{H^+}H_{aq}^+ = -\mathrm{Log}_{10}\frac{1000\gamma_{H^+}H_{air}^+}{ALWC_i+ALWC_o} \cong -\mathrm{Log}_{10}\frac{1000\gamma_{H^+}H_{air}^+}{ALWC_i} \quad (1)$$

where γ_{H^+} is the activity coefficient of hydronium ion (assumed to be unity, following the default ISORROPIA-II setting, Fountoukis and Nenes, 2007), H_{aq}^+ (mol L^{-1}) is the concentration of hydronium ion in particle liquid water, H_{air}^+ (μg m^{-3}) is the mass concentration of hydronium ion in air, and $ALWC_i$ and $ALWC_o$ (μg m^{-3}) is the water concentration of bulk particle related to inorganic and organic species, respectively. ~~Since the pH predictions were insensitive to $ALWC_o$ according to previous studies (Battaglia Jr et al., 2019; Guo et al., 2015; Ding et al., 2019), we only consider the portion of $ALWC_i$ in pH calculation.~~ Given the limited influence of $ALWC_o$ on pH calculation reported in previous studies (Guo et al., 2015; Zhou et al., 2022) and the lack of organic hygroscopicity (κ_{org}) measurements in this study, we primarily used $ALWC_i$ for pH calculation. To further assess this assumption, we estimated $ALWC_o$ using a global mean κ_{org} of 0.12 (Pöhlker et al., 2023), following the equation (Guo et al., 2015):

$$ALWC_o = \frac{m_{org}\rho_w}{\rho_{org}} \frac{\kappa_{org}}{(\frac{1}{RH}-1)} \quad (2)$$

where m_{org} is the mass concentration of organic aerosol, ρ_w is the density of water (ρ_w = 1.0 g cm^{-3}), ρ_{org} is the density of organics (ρ_{org} = 1.4 g cm^{-3}; Guo et al., 2015).

The estimated $ALWC_o$ averaged 11.2 ± 18.1 μg m^{-3}, substantially lower than $ALWC_i$ (43.2 ± 75.5 μg m^{-3}). When $ALWC_o$ was included in the pH calculations, the resulting pH values showed a strong correlation with those calculated without $ALWC_o$ (R^2 = 0.99; Fig. S1), with the pH increasing slightly from 3.82 ± 0.96 to 3.96 ± 0.93 (~4% change). This suggests that the influence of $ALWC_o$ on the estimated pH in our dataset is relatively limited. It should also be noted that alkaline cations (e.g., Ca^{2+}, Mg^{2+}, Na^+, K^+) were not included in our simulations due to the lack of measurements, which may lead to a systematic underestimation of aerosol pH (Guo et al., 2017).

Previous studies have shown that pH predictions from thermodynamic models can exhibit substantial biases when operated in the "reverse" mode (Hennigan et al., 2015; Song et al., 2018). Meanwhile, H^+ is inherently unstable under efflorescent particle conditions (Hennigan et al., 2015). To minimize these uncertainties, we ran ISORROPIA II in "forward" mode and "metastable" state, assuming fully deliquesced aerosols without solid formation. Furthermore, only data with RH > 30% were included to avoid unrealistic pH values arising from misestimated ALWC at low RH, as noted in previous studies (Liu et al., 2017; Ding et al., 2019; Xie et al., 2020).

The accuracy of the thermodynamic simulation and the resulting pH prediction was evaluated by comparing the predicted and observed NH_3/NH_4^+ partitioning (Guo et al., 2016). As shown in Fig. ~~S1~~S2, the modeled values agree well with the measurements (R^2 = 0.82-0.96, slope = 0.80-1.07), indicating that the performance of the ISORROPIA II model is satisfactory for this study.

2.3 Explainable machine learning model and interpretation

An explainable machine-learning model based on the extreme gradient boosting (XGBoost) algorithm was developed (Gui et al., 2020; Peng et al., 2023; Cai et al., 2025). The input features included chemical indicators such as excess ammonia (Excess NHx, calculated as described in

Text S2), nitrate-to-sulfate mass ratio (N/S ratio), and PM_1 mass loading, together with meteorological parameters (temperature and RH). Aerosol pH calculated using ISORROPIA II served as the target variable. The derived variables (Excess NHx, N/S ratio, and PM_1) were chosen as proxies for neutralization capacity, nitrate/sulfate dominance, and pollution level, respectively, providing a more generalized perspective on how aerosol chemical properties are associated with pH rather than focusing on absolute concentrations of individual species. The correlation matrix (Fig. S3) showed weak correlations among all feature pairs ($R^2 < 0.2$), indicating that multicollinearity is negligible and that the features can be treated as relatively independent predictors in the XGBoost-SHAP analysis.~~These features were selected because they collectively capture key meteorological and chemical characteristics potentially influencing aerosol pH, according to previous studies (Liu et al., 2017; Zheng et al., 2020; Zhou et al., 2022)~~. The dataset was randomly divided into training (70%) and testing (30%) subsets. A 10-fold cross-validation procedure, repeated five times, was applied to ensure robust generalization and reduce overfitting (Qin et al., 2022; Peng et al., 2023). Model performance was evaluated using the root mean square error (RMSE, 0.12), mean absolute error (MAE, 0.08), and coefficient of determination ($R^2 = 0.98$; Fig. ~~S2~~S4). This high performance suggests that the model has adequately learned the dominant relationships embedded in the thermodynamic behavior and providing a reliable basis for the subsequent SHAP-based interpretation. To evaluate the temporal generalizability of the model, we additionally performed leave-one-month-out cross-validation, in which each month was iteratively held out as the test set while the remaining months were used for training (Bergmeir and Benítez, 2012; Chen et al., 2021). This validation yielded an average R^2 of 0.86 ± 0.13 (Table S1), suggesting that the model maintains good predictive performance across independent time periods and captures generalizable relationships rather than temporally correlated patterns.

The Shapley additive explanations (SHAP) algorithm (Lundberg et al., 2020) was employed to interpret model outputs and quantify the relative importance of each predictor (the XGBoost–SHAP framework). SHAP assigns each input variable a contribution to the model output, capturing potential nonlinear effects. For each sample, the predicted value can be expressed as:

$$f(x_i)=\phi_0(f,x)+\sum_{ij=1}^{M}\phi_j(f,x_i) \qquad (23)$$

where $f(x_i)$ is the predicted value for sample (x_i) with M features, $\phi_0(f, x)$ is the base value (expected output), and $\phi_j(f, x_i)$ is the SHAP value of feature j (Lundberg et al., 2020). In addition to quantifying the marginal contribution of individual features, the SHAP framework was extended to compute pairwise interaction values using the Shapley interaction index from cooperative game theory (Lundberg et al., 2020). This approach decomposes each prediction into nonlinear main effects and interaction effects, providing more informative local explanations for individual predictions (Hou et al., 2022; Qi et al., 2025). By isolating these terms at the sample level, SHAP interaction analysis characterizes how combinations of predictors jointly influence model outputs, patterns that may not be captured by marginal SHAP values alone.

Unlike conventional thermodynamic sensitivity analyses that typically vary one factor at a time (or examine pairwise effects) under fixed conditions (Guo et al., 2017; Ding et al., 2019; Xie et al., 2019; Wei et al., 2023), the XGBoost-SHAP framework diagnoses nonlinear and interactive pH responses from observational data in a sample-level, data-driven manner. It characterizes sample-level heterogeneity, quantifies the relative importance of different factors, and identifies regime-dependent behaviors, providing complementary insights into pH variation under the complex, co-varying conditions of the real atmosphere. We emphasize that the XGBoost–SHAP approach serves primarily as a statistical and interpretable tool, providing a data-driven decomposition of how each predictor contributes to pH variations, rather than identifying independent causal mechanisms.

Centered individual conditional expectation (c-ICE) plots were also employed to examine nonlinear effects and feature interactions. Individual conditional expectation (ICE) curves describe how model predictions change as a single feature varies while all other features are held fixed, thereby preserving sample-specific trajectories and capturing the heterogeneity of feature effects across observations (Wei et al., 2022). However, the interpretation of ICE curves can be hindered by substantial vertical offsets among individual curves. To address this, c-ICE curves are constructed by centering each ICE curve at a reference point, effectively removing

vertical shifts and highlighting the variation in predictions attributable to the feature itself (Yang et al., 2023; Yang et al., 2024). Divergences or non-parallel patterns among c-ICE curves indicate that the effect of a given feature depends on the values of other predictors, providing visual evidence of feature interactions at the sample-specific level.

3. Results and discussion

3.1 Relative importance of key factors for overall pH variability

Time series of meteorological and chemical measurements, together with ISORROPIA-derived pH and ALWC, are shown in Fig. 1. The average aerosol pH value was 3.8 ± 0.96, with the samples predominantly falling within the range of 1.5–6.0 (Fig. S5). This range is comparable to previous observations in urban Beijing (Ding et al., 2019; Xie et al., 2020)~~Aerosol pH ranged from 0.8 to 6.7 (average of 3.8), comparable to previous observations in North China (Ding et al., 2019; Xie et al., 2020; Wei et al., 2023)~~, and displayed pronounced seasonal and synoptic variability. Excess NHx remained positive, indicating strongly ammonia-rich conditions (Song et al., 2018), while the N/S ratio spanned from sulfate-dominant to nitrate-dominant states. The temporal variability in chemical composition and meteorology provides a representative dataset for quantifying their relative contributions to aerosol acidity variation across diverse environmental conditions.

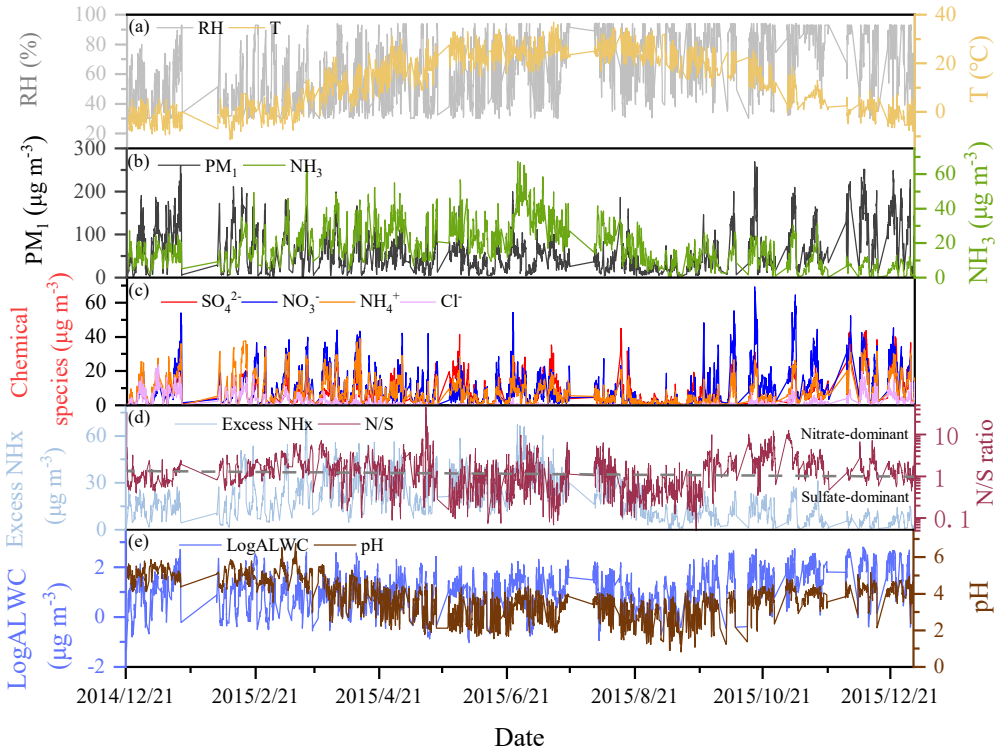

Figure 1. Time series of meteorological and chemical measurements and derived model variables during the sampling period. Panels show (a) temperature and relative humidity (RH), (b) mass concentrations of PM_1 and gaseous NH_3, (c) inorganic species including SO_4^{2-}, NO_3^-, NH_4^+, and Cl^-, (d) Excess NHx and the nitrate-to-sulfate mass ratio (N/S ratio), and (e) aerosol pH and aerosol liquid water content (ALWC) calculated by ISORROPIA II.

The mean absolute SHAP values provide a global ranking of predictors contributing to aerosol pH variability across the observation period (Fig. ~~S3~~S6). Temperature emerges as the most significant factor, followed by Excess NHx, N/S ratio, RH, and PM_1 mass loading. The dominant role of temperature in explaining the overall pH variability is consistent with previous thermodynamic sensitivity analyses (Jia et al., 2020; Tao and Murphy, 2021). Examining each predictor in detail (Fig. 2), SHAP values show a strong, monotonic negative contribution of temperature, with low-temperature conditions corresponding to higher pH. This pattern aligns with thermodynamic predictions, in which lower temperatures favor ammonia partitioning into the particle phase and higher aerosol liquid water, both likely elevate pH (Ding et al., 2019; Jia et al., 2020). Both higher Excess NHx and elevated N/S ratio correspond to positive SHAP

contributions, consistent with previous thermodynamic analyses suggesting more ammonia-rich and nitrate-rich conditions generally enhance aerosol neutralization and shift pH upward (Wang et al., 2020; Xie et al., 2020). RH, however, exhibits a more complex pattern, with positive SHAP values occurring across both low- and high-RH conditions, reflecting the strong condition dependence of RH contributions. Finally, as the least influential factor, PM_1 mass loading also contributes positively to aerosol pH, with higher PM_1 concentration being associated with larger SHAP values.

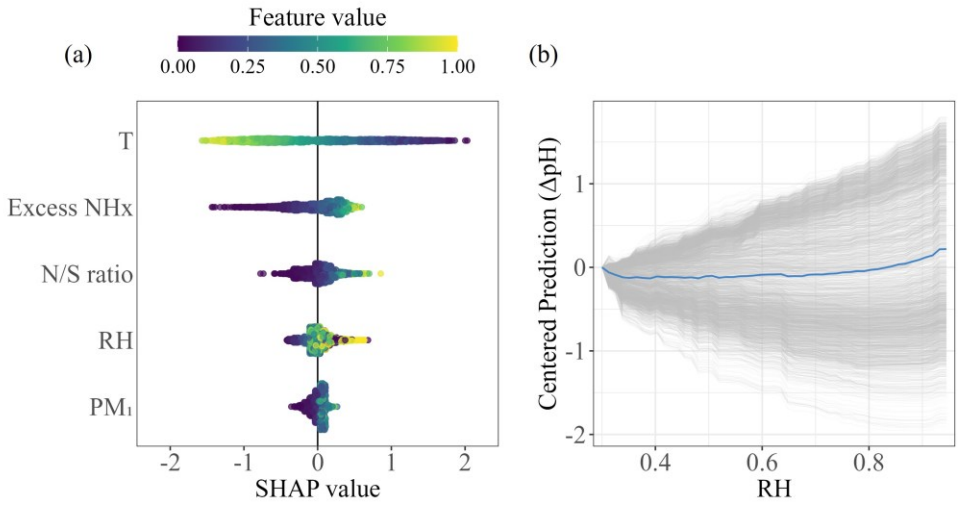

Figure 2. ~~Global SHAP summary plot showing the relative importance and overall contributions of individual features, including temperature (T, °C), Excess NHx (μg m^{-3}), nitrate-to-sulfate mass ratio (NtoSratio), PM_1 mass loading (μg m^{-3}), and RH, to aerosol pH (a), and c-ICE curves illustrating sample-specific effects of each feature on aerosol pH (gray lines) along with their averaged responses (blue line) (b).~~ Global SHAP summary plot (a) showing the relative importance of temperature (T, °C), RH, Excess NHx (μg m^{-3}), N/S ratio, and PM_1 mass loading (μg m^{-3}) to aerosol pH. Panel (b) shows c-ICE curves of RH, with gray lines representing sample-specific effects and the blue line showing the averaged response.

The c-ICE analysis further resolves variable-specific responses (Fig. 2b and Fig. S7). For temperature, Excess NHx, N/S ratio, and PM_1 mass, c-ICE curves generally align with global SHAP trends, indicating their largely monotonic influences on predicted pH across samples

(Fig. S7). In particular, the average decreasing trend of pH with temperature corresponds to a reduction of ~0.6 units per 10 °C increase, consistent with the ISORROPIA II thermodynamic sensitivity test results (Fig. ~~S4~~S8). For Excess NHx, increases at lower concentrations correspond to substantial rises in predicted pH, with a 20 μg m^{-3} increase associated with a nearly 1.5 units rise in pH, while the response flattens at higher concentrations, implying decreasing sensitivity (Liu et al., 2017; Ding et al., 2019). RH, in contrast, exhibits markedly different behavior (Fig. 2b). The c-ICE curves reveal pronounced sample-to-sample variability, with approximately half of the samples showing positive pH responses to increasing RH and the remaining samples showing negative responses. This pronounced heterogeneity indicates that the RH contributions are highly condition-dependent, strongly modulated by interactions with other variables, which may be overlooked by traditional sensitivity tests based on average conditions (Fig. S4) and warrants further investigation.

3.2 Regime-dependent RH interactions with other factors

Pairwise interactions (Lundberg et al., 2020; Hou et al., 2022; Qi et al., 2025) between meteorological and chemical factors were analyzed to assess their combined contributions to pH prediction (Fig. 3 and Fig. ~~S5~~S9). RH-related interactions are generally stronger and more systematic~~systematical~~ than those of other variable pairs, consistent with the pronounced condition-dependent c-ICE behavior of RH discussed above.

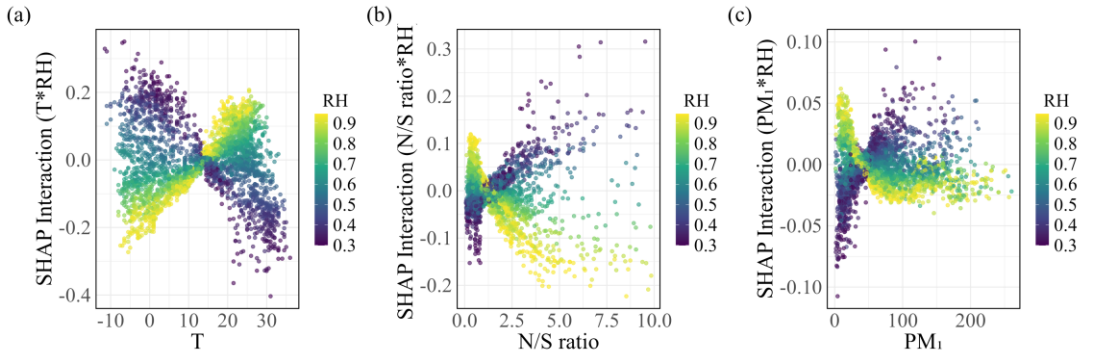

Figure 3. ~~SHAP interaction plots illustrating the joint effects of RH with temperature (°C) (a), N/S mass ratio (b), and PM_1 mass loading (μg m^{-3}) (c) on aerosol pH prediction. The color scale represents RH, and the SHAP interaction values indicate the direction and magnitude of RH modulation on predicted pH under different regimes.~~ SHAP interaction plots showing the joint

contributions of RH with temperature (T, °C) (a), N/S ratio (b), and PM_1 mass loading (μg m^{-3}) (c) to aerosol pH predictions. The color scale represents RH, and the SHAP interaction values indicate the direction and magnitude of the interactive contributions to pH across different regimes.

As two key meteorological parameters, temperature and RH exhibit strong statistical interactions in pH prediction, with opposite patterns across different regimes (Fig. 3a). The thresholds were identified from inflection points in the SHAP interaction plots, where the SHAP interaction values crossed zero and the direction of the RH–pH relationship reversed. The robustness of these approximate thresholds was supported by sensitivity tests under different random seeds and train/test split ratios (Fig. S10 and Fig. S11). At temperatures below ~15 °C, higher RH is associated with lower pH values in the model prediction at a given temperature, with RH–temperature interaction SHAP values showing a maximum decrease from approximately 0.30 to −0.25. In contrast, at temperatures above ~15 °C, this interaction reverses, with higher RH corresponding to higher predicted pH. Specifically, higher predicted aerosol acidity occurs under both low-temperature–high-RH and high-temperature–low-RH conditions, whereas the opposite combinations correspond to lower acidity.

~~This regime-dependent behavior can be explained by the coupled influence of temperature and RH on secondary inorganics formation, gas particle partitioning and aerosol water uptake, which together modulate the balance between H^+ input and dilution (Ding et al., 2019; Tao et al., 2025).~~ This regime-dependent association behavior identified by SHAP model is consistent with the coupled influence of temperature and RH on gas–particle partitioning, aerosol water uptake, and secondary inorganic formation, which together may modulate the balance between H^+ input and dilution—two key factors related to different pH variations (Ding et al., 2019; Tao et al., 2025). According to previous studies, ~~Under~~ under low-temperature conditions, thermodynamic equilibrium favors the partitioning of semi-volatile species into the particle phase (Guo et al., 2015). ~~Elevated RH could not only increase ALWC but also facilitate heterogeneous reactions of gaseous precursors to form secondary inorganic aerosols, accompanied by H^+ accumulation (Liu et al., 2017; Ding et al., 2019).~~ Elevated RH could not only enhance aerosol water uptake but also facilitate heterogeneous reactions of gaseous

precursors to form secondary inorganic aerosols, accompanied by H^+ accumulation likely primary from the dissociation of HNO_3 upon aqueous uptake and the multiphase oxidation of SO_2 (Wang et al., 2016; Liu et al., 2017). Consistently, ~~As~~ as shown in Fig. 4, at temperatures below 15 °C, both H^+ and ALWC increased with RH, accompanied by a decrease in pH. This likely suggests that ~~That means~~ under low-temperature conditions, enhanced inorganic aerosol formation and associated H^+ accumulation likely outweigh the concurrent increase in ALWC and its dilution effect, which might be associated with increased aerosol acidity~~resulting in increased aerosol acidity~~. In contrast, at higher temperatures, elevated RH still enhances aerosol water uptake. However, enhanced volatilization of semi-volatile species shifts gas–particle partitioning towards the gas phase, likely reducing the availability of these precursors for aqueous-phase reactions and thereby limiting H^+ generation in the particle phase (Ding et al., 2019; Tao et al., 2025). As a result, the increased aerosol water at high RH predominantly exerts a dilution effect. ~~enhanced volatilization shifts gas-particle partitioning towards the gas phase, likely limiting H^+ accumulation in particles (Ding et al., 2019; Tao et al., 2025).~~ Consistently, at temperatures above 15 °C, H^+ slightly decreased with increasing RH, while ALWC continued to increase and pH correspondingly increased (Fig. 4). In this regime, the dominant effect of higher RH ~~should~~ might be the enhancement of ALWC dilution, which is likely associated with ~~resulting in~~ lower aerosol acidity. Temperature therefore likely modulates whether RH-driven H^+ accumulation or ALWC dilution prevails, which may be associated with~~producing~~ opposite RH sensitivities across different regimes.

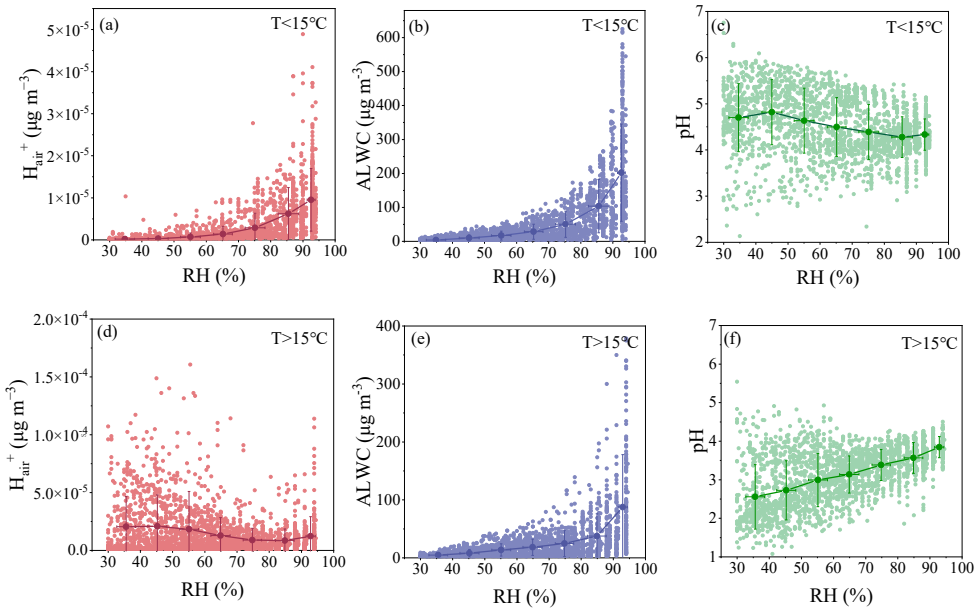

Figure 4. Scatter plots of H_{air}^+ (μg m^{-3}), ALWC (μg m^{-3}), and pH versus RH, along with their average variation trends with RH for temperature lower than 15℃ (a, b, c), and higher than 15℃ (d, e, f), respectively.

Strong statistical interactions were also observed between RH and chemical parameters, including the N/S ratio and PM_1 mass loading, both exhibiting clear threshold-dependent regime shifts (Fig. 3b, c). Under sulfate-dominant conditions (N/S ratio < ~1.25), higher RH tends to be associated with higher predicted pH, whereas this pattern reverses under nitrate-dominant conditions (N/S ratio > ~1.25), where higher RH is associated with lower predicted pH. A similar regime-dependent behavior is evident for PM_1 mass loading, with RH showing a positive association with ~~with RH exerting a positive contribution to~~ predicted pH at low PM_1 concentrations (< ~50 μg m^{-3}) but an increasingly negative ~~contribution~~ association at higher loadings (> ~50 μg m^{-3}). The evolution of H^+ and ALWC with RH across different N/S ratio and PM_1 loading regimes was also analyzed (Fig. 5). ~~Consistently, under~~ Under sulfate-dominant or low-mass conditions (N/S < 1.25 or PM_1 < 50 μg m^{-3}), H^+ slightly decreased while ALWC continued to increase with increasing RH, suggesting that dilution by aerosol water likely outweighed H^+ input, which might be associated with elevated pH~~such that dilution by aerosol water likely outweighed, resulting in elevated pH~~ (Fig. 5). In contrast, under nitrate-

dominant or high-mass conditions (N/S > 1.25 or PM_1 > 50 μg m^{-3}), concurrent enhancements in both H^+ and ALWC were observed with increasing RH, accompanied by a slight decrease in pH, reflecting that H^+ accumulation likely outweighed the concurrent dilution by ALWC.

These patterns are consistent with the complex multiphase chemical processes among different regimes (Wang et al., 2016; Xie et al., 2020; Wang et al., 2025). ~~These might be related to the complex multiphase chemical processes among different regimes.~~ Under cleaner conditions with low PM_1 loading, elevated RH is expected to substantially enhance ALWC. At the same time, secondary inorganic aerosol formation might be limited by the low availability of precursor gases. As a result, the additional aerosol water may act mainly through dilution, which is likely associated with higher pH. ~~Under cleaner periods with low PM_1 loading, elevated RH substantially increases ALWC while secondary inorganic aerosol formation remains relatively limited due to lower precursor concentrations.~~ In contrast, under high-PM_1 conditions, the abundant particle surface area and elevated ionic strength may create favorable media for multiphase reactions (Mekic et al., 2021). The ~~under higher PM_1 loading, abundant particles provide extensive reaction media, and~~ enhanced water uptake at elevated~~high~~ RH ~~could~~ likely facilitate heterogeneous/aqueous-phase formation of secondary inorganic aerosols (Wang et al., 2025), thereby promoting additional acidity production that may offset or outweigh the water dilution effect (Fig.5). ~~The resulting H^+ accumulation likely outweighs the water dilution effect and decreases pH (Fig. 5).~~ Regarding the RH–N/S interaction, according to previous studies, NH_3 first neutralizes sulfuric acid and subsequently reacts with HNO_3, and aerosol pH generally decreases with increasing sulfate but increases with increasing nitrate (Ding et al., 2019; Xie et al., 2020). Under sulfate-dominant conditions (low N/S), increased RH enhances the aqueous uptake of NH_3, partially neutralizing existing acidity and mainly promoting the formation of NH_4NO_3 (Fig. ~~S6~~S12), which is therefore likely associated with an increase in pH. In contrast, under nitrate-dominant conditions (high N/S), the increase in sulfate mass with RH is more pronounced than that of nitrate (Fig. ~~S6~~S12). This likely suggests that~~That means~~ under this regime, the efficient aqueous medium is likely more favorable for sulfate production (e.g., through multiphase oxidation of SO2 and NOx) (Wang et al., 2016). This process likely introduces additional acidity to the particle phase and is likely associated with a decrease in pH

~~leads to a decrease in pH again~~. These results underscore the importance of multiphase chemical processes in influencing aerosol pH variation under different environmental regimes.

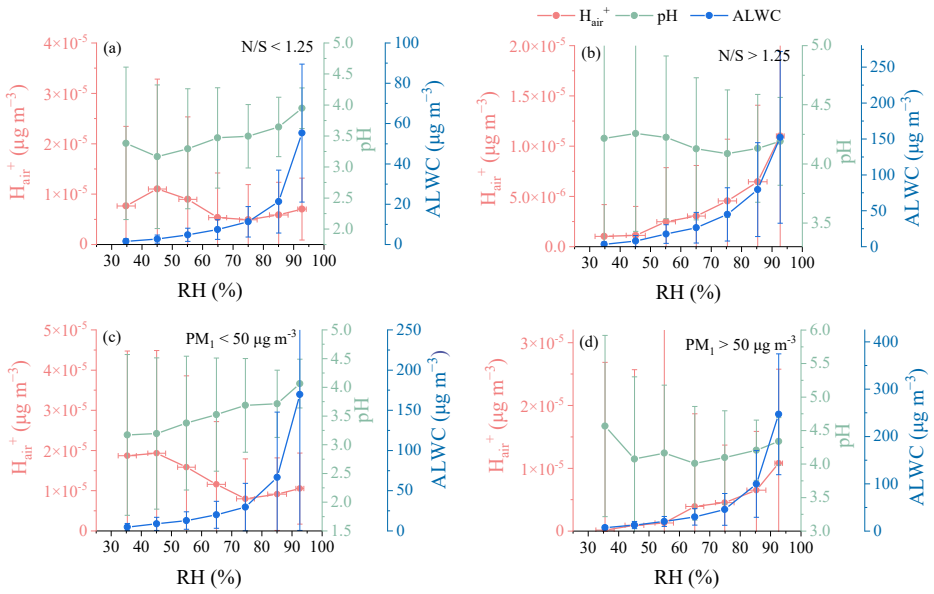

Figure 5. Variations of H_{air}^+ (μg m^{-3}), ALWC (μg m^{-3}), and pH as a function of RH under different environmental conditions: (a) N/S mass ratio < 1.25, (b) N/S mass ratio > 1.25, separated by the nitrate-to-sulfate mass ratio; (c) PM_1 mass loading < 50 μg m^{-3}, and (d) PM_1 mass loading > 50 μg m^{-3}, separated by PM_1 mass loading levels.

3.3 Seasonal patterns of RH-associated variability in aerosol pH

The regime-dependent relationship between aerosol pH and RH identified by SHAP provides a coherent framework for interpreting the seasonal patterns observed during our ammonia-rich campaign. For example, RH generally showed negative association with~~contributions to~~ pH in winter, whereas in summer it exerted a positive association with pH and ranked as the largest contributor to pH variability (Fig. 6). This seasonal reversal aligns with the RH–temperature/chemical interactions discussed above. Low winter temperatures (<10 °C) place pH within regimes where elevated RH is linked to higher aerosol acidity, whereas higher summer temperatures (12–40 °C) shift pH into regimes where higher RH is associated with lower acidity (Fig. ~~S7~~S13). In addition, lower PM_1 mass loadings in summer (with a peak frequency at ~30 μg m^{-3}) compared to winter (with a peak frequency at ~90 μg m^{-3}) align with the positive RH–pH relationship under low PM_1 conditions and the negative relationship under

high PM_1 conditions discussed above (Fig. ~~S7~~S13). Such seasonally contrasting RH–pH associations also agree with thermodynamic sensitivity analyses conducted by Ding et al. (2019), supporting the consistency~~reinforcing the plausibility~~ of the interaction patterns identified here. Overall, these results highlight that RH-related pH variability should be interpreted in conjunction with temperature and the prevailing chemical buffering regime.–

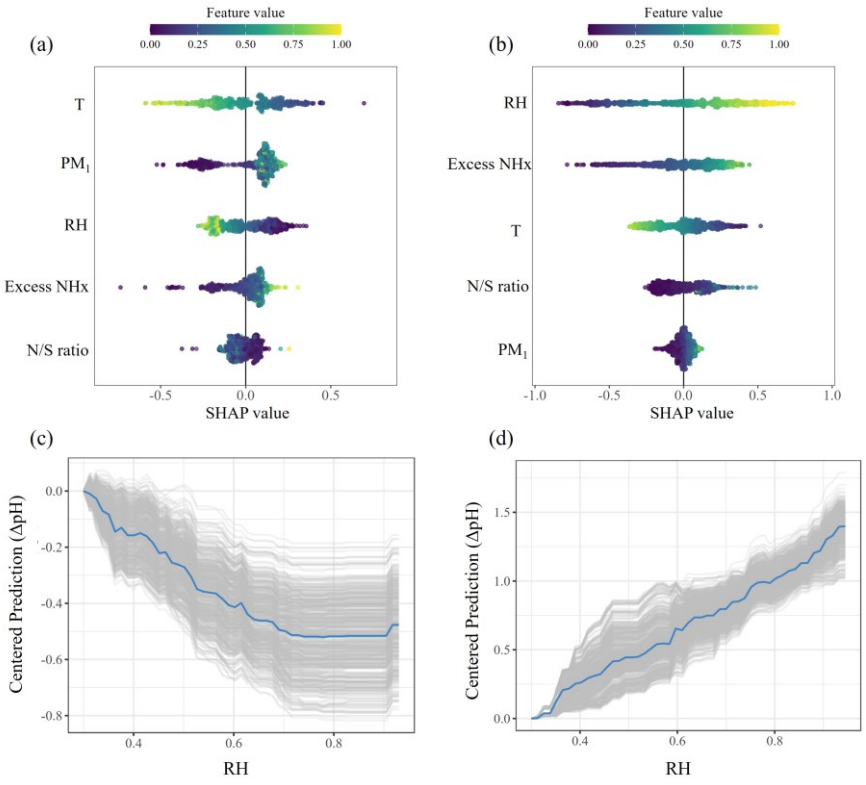

Figure 6. SHAP values showing the relative importance of input features for aerosol pH during the winter (a) and summer (b) periods, illustrating their contributions to pH variability. c-ICE curves (gray lines) and their averages (blue line) depicting the relationships between RH and pH between winter (c) and summer (d).

4. Conclusions and implications

In this study, we provide a comprehensive, data-driven assessment of aerosol pH variability in an ammonia-rich urban atmosphere by integrating machine learning, field observations, and thermodynamic modeling. Our results indicate that aerosol pH is closely associated with both meteorological conditions and chemical composition. Temperature shows a dominant negative contribution, whereas excess ammonia, N/S ratio, and PM_1 mass loading are positively

associated with pH. The contribution of RH, however, is highly regime-dependent, with its contribution reversing under different combinations of temperature, chemical composition, and aerosol loading. By quantifying threshold boundaries, visualizing regime transitions, and resolving sample-level variability, the SHAP framework complements traditional thermodynamic analyses and provides quantitative insights into the conditions under which RH is linked to higher or lower aerosol pH.

The thresholds and interaction patterns identified here are based on observations at a single urban site in Beijing and may therefore reflect local meteorology and emission characteristics. ~~Nevertheless, this approach provides a quantitative framework for understanding and predicting aerosol pH responses under evolving atmospheric environments.~~Nevertheless, this approach provides a quantitative framework for identifying the nonlinear relationships between pH and complex coupled environmental parameters. ~~In China's increasingly ammonia-rich atmosphere, aerosol pH response generally falls within a flattened regime, exhibiting weak sensitivity to further increases in ammonia. Under such conditions, meteorological factors, together with particle properties such as total mass loading and the relative contributions of sulfate and nitrate, will jointly modulate aerosol acidity. Ongoing decreases in particle mass and the gradual shift from sulfate-dominated to nitrate-dominated composition in recent years are expected to substantially modify aerosol buffering properties.~~ In China's evolving atmosphere, meteorological factors, together with variable particle properties, may jointly modulate aerosol acidity. ~~Additionally, d~~Distinct environment conditions not considered in this study, such as coastal regions influenced by sea salt (Wang et al., 2022; Xu et al., 2025) and dust-affected areas enriched in alkaline metals (Shi et al., 2019; Huang et al., 2020), likely also exert important contributions to pH variation. ~~may also exert important roles in pH variation.~~ Extending this SHAP-based analytical framework to diverse atmospheric conditions would be a valuable direction for future research to further understand the regime-dependent pH variations across different environments. ~~Extending this SHAP-based analytical framework to diverse atmospheric conditions will enable a more general characterization of pH regimes in ammonia-rich environments and improve predictive capability under a wide range of future scenarios.~~

Data availability. The data used in this study can be obtained from https://doi.org/10.5281/zenodo.19585092 (Duan and Wang, 2026). It is also available from the corresponding author upon request.

Author contributions. RJH designed the study. JD and TW performed the data analysis and interpretation, with contributions from JYR, HBZ, and WX. JD, TW and RJH wrote the manuscript, and all authors contributed to scientific discussions and revision of the manuscript.

Competing interests. The authors declare that they have no conflict of interest.

Acknowledgements. This work was supported by the National Natural Science Foundation of China (NSFC) (grant no. 42525301, 42430708, and 42577125), the Key Research Program of Frontier Sciences from the Chinese Academy of Sciences (ZDBS-LY-DQC001), the Innovation Capability Support Program of Shaanxi (2024RS-CXTD-40), and the New Cornerstone Science Foundation through the XPLORER PRIZE.

Reference

Battaglia Jr, M. A., Weber, R. J., Nenes, A., and Hennigan, C. J.: Effects of water-soluble organic carbon on aerosol pH, Atmos. Chem. Phys., 19, 14607-14620, 10.5194/acp-19-14607-2019, 2019.

Bergmeir, C. and Benítez, J. M.: On the use of cross-validation for time series predictor evaluation, Inform. Sciences, 191, 192-213, 10.1016/j.ins.2011.12.028, 2012.

Cai, A., Wang, L., Zhang, Y., Wu, H., Zhang, H., Guo, R., and Wu, J.: Uncovering the multiple socio-economic driving factors of carbon emissions in nine urban agglomerations of China based on machine learning, Energy, 319, 134859, 10.1016/j.energy.2025.134859, 2025.

Cao, Y., Zhang, Z., Xiao, H., Xie, Y., Liang, Y., and Xiao, H.: How aerosol pH responds to nitrate to sulfate ratio of fine-mode particulate, Environ Sci Pollut Res Int, 27, 35031-35039, 10.1007/s11356-020-09810-0, 2020.

Chen, C.-C., Wang, Y.-R., Yeh, H.-Y., Lin, T.-H., Huang, C.-S., and Wu, C.-F.: Estimating monthly $PM_{2.5}$ concentrations from satellite remote sensing data, meteorological variables, and land use data using ensemble statistical modeling and a random forest approach,

Environ. Pollut., 291, 118114, 10.1016/j.envpol.2021.118114, 2021.

Clegg, S. L., Seinfeld, J. H., and Brimblecombe, P.: Thermodynamic modelling of aqueous aerosols containing electrolytes and dissolved organic compounds, Journal of aerosol science, 32, 713-738, 2001.

Dai, T., Dai, Q., Ding, J., Liu, B., Bi, X., Wu, J., Zhang, Y., and Feng, Y.: Measuring the Emission Changes and Meteorological Dependence of Source-Specific BC Aerosol Using Factor Analysis Coupled With Machine Learning, J. Geophys. Res.-Atmos., 128, e2023JD038696, 10.1029/2023jd038696, 2023.

Ding, J., Zhao, P., Su, J., Dong, Q., Du, X., and Zhang, Y.: Aerosol pH and its driving factors in Beijing, Atmos. Chem. Phys., 19, 7939-7954, 10.5194/acp-19-7939-2019, 2019.

Duan, X., Zheng, G., Chen, C., Zhang, Q., and He, K.: Driving factors of aerosol acidity: a new hierarchical quantitative analysis framework and its application in Changzhou, China, Atmos. Chem. Phys., 25, 3919-3928, 10.5194/acp-25-3919-2025, 2025.

Fountoukis, C. and Nenes, A.: ISORROPIA II: a computationally efficient thermodynamic equilibrium model for K^+–Ca^{2+}–Mg^{2+}–NH_4^+–Na^+–SO_4^{2-}–NO_3^-–Cl^-–H_2O aerosols, Atmos. Chem. Phys., 7, 4639-4659, 2007.

Fu, Z., Cheng, L., Ye, X., Ma, Z., Wang, R., Duan, Y., Juntao, H., and Chen, J.: Characteristics of aerosol chemistry and acidity in Shanghai after PM(2.5) satisfied national guideline: Insight into future emission control, Sci. Total Environ., 827, 154319, 10.1016/j.scitotenv.2022.154319, 2022.

Giorio, C., D'Aronco, S., Di Marco, V., Badocco, D., Battaglia, F., Solda, L., Pastore, P., and Tapparo, A.: Emerging investigator series: aqueous-phase processing of atmospheric aerosol influences dissolution kinetics of metal ions in an urban background site in the Po Valley, Environ. Sci.: Process. Impacts, 24, 884-897, 10.1039/d2em00023g, 2022.

Grange, S. K., Carslaw, D. C., Lewis, A. C., Boleti, E., and Hueglin, C.: Random forest meteorological normalisation models for Swiss PM10 trend analysis, Atmos. Chem. Phys., 18, 6223-6239, 10.5194/acp-18-6223-2018, 2018.

Gui, K., Che, H., Zeng, Z., Wang, Y., Zhai, S., Wang, Z., Luo, M., Zhang, L., Liao, T., Zhao, H., Li, L., Zheng, Y., and Zhang, X.: Construction of a virtual PM(2.5) observation

network in China based on high-density surface meteorological observations using the Extreme Gradient Boosting model, Environ. Int., 141, 105801, 10.1016/j.envint.2020.105801, 2020.

Guo, H., Liu, J., Froyd, K. D., Roberts, J. M., Veres, P. R., Hayes, P. L., Jimenez, J. L., Nenes, A., and Weber, R. J.: Fine particle pH and gas–particle phase partitioning of inorganic species in Pasadena, California, during the 2010 CalNex campaign, Atmos. Chem. Phys., 17, 5703-5719, 10.5194/acp-17-5703-2017, 2017.

Guo, H., Sullivan, A. P., Campuzano-Jost, P., Schroder, J. C., Lopez-Hilfiker, F. D., Dibb, J. E., Jimenez, J. L., Thornton, J. A., Brown, S. S., Nenes, A., and Weber, R. J.: Fine particle pH and the partitioning of nitric acid during winter in the northeastern United States, J. Geophys. Res.-Atmos., 121, 10-355, 10.1002/2016jd025311, 2016.

Guo, H., Xu, L., Bougiatioti, A., Cerully, K. M., Capps, S. L., Hite, J. R., Carlton, A. G., Lee, S. H., Bergin, M. H., Ng, N. L., Nenes, A., and Weber, R. J.: Fine-particle water and pH in the southeastern United States, Atmos. Chem. Phys., 15, 5211-5228, 10.5194/acp-15-5211-2015, 2015.

Hennigan, C. J., Izumi, J., Sullivan, A. P., Weber, R. J., and Nenes, A.: A critical evaluation of proxy methods used to estimate the acidity of atmospheric particles, Atmos. Chem. Phys., 15, 2775-2790, 10.5194/acp-15-2775-2015, 2015.

Hou, L., Dai, Q., Song, C., Liu, B., Guo, F., Dai, T., Li, L., Liu, B., Bi, X., Zhang, Y., and Feng, Y.: Revealing Drivers of Haze Pollution by Explainable Machine Learning, Environ. Sci. Technol. Lett., 9, 112-119, 10.1021/acs.estlett.1c00865, 2022.

Huang, R. J., Duan, J., Li, Y., Chen, Q., Chen, Y., Tang, M., Yang, L., Ni, H., Lin, C., Xu, W., Liu, Y., Chen, C., Yan, Z., Ovadnevaite, J., Ceburnis, D., Dusek, U., Cao, J., Hoffmann, T., and O'Dowd, C. D.: Effects of NH(3) and alkaline metals on the formation of particulate sulfate and nitrate in wintertime Beijing, Sci. Total Environ., 717, 137190, 10.1016/j.scitotenv.2020.137190, 2020.

Jia, S., Chen, W., Zhang, Q., Krishnan, P., Mao, J., Zhong, B., Huang, M., Fan, Q., Zhang, J., Chang, M., Yang, L., and Wang, X.: A quantitative analysis of the driving factors affecting seasonal variation of aerosol pH in Guangzhou, China, Sci. Total Environ., 725, 138228,

10.1016/j.scitotenv.2020.138228, 2020.

Liu, M., Song, Y., Zhou, T., Xu, Z., Yan, C., Zheng, M., Wu, Z., Hu, M., Wu, Y., and Zhu, T.: Fine particle pH during severe haze episodes in northern China, Geophys. Res. Lett., 44, 5213-5221, 10.1002/2017gl073210, 2017.

Lundberg, S. M., Erion, G., Chen, H., DeGrave, A., Prutkin, J. M., Nair, B., Katz, R., Himmelfarb, J., Bansal, N., and Lee, S. I.: From Local Explanations to Global Understanding with Explainable AI for Trees, Nat. Mach. Intell., 2, 56-67, 10.1038/s42256-019-0138-9, 2020.

Maasikmets, M., Teinemaa, E., Kaasik, A., and Kimmel, V.: Measurement and analysis of ammonia, hydrogen sulphide and odour emissions from the cattle farming in Estonia, Biosyst. Eng., 139, 48-59, 10.1016/j.biosystemseng.2015.08.002, 2015.

Mekic, M. and Gligorovski, S.: Ionic strength effects on heterogeneous and multiphase chemistry: Clouds versus aerosol particles, Atmos. Environ., 244, 117911, 10.1016/j.atmosenv.2020.117911, 2021.

Mo, Y., Li, J., Liu, J., Zhong, G., Cheng, Z., Tian, C., Chen, Y., and Zhang, G.: The influence of solvent and pH on determination of the light absorption properties of water-soluble brown carbon, Atmos. Environ., 161, 90-98, 10.1016/j.atmosenv.2017.04.037, 2017.

Myriokefalitakis, S., Ito, A., Kanakidou, M., Nenes, A., Krol, M. C., Mahowald, N. M., Scanza, R. A., Hamilton, D. S., Johnson, M. S., Meskhidze, N., Kok, J. F., Guieu, C., Baker, A. R., Jickells, T. D., Sarin, M. M., Bikkina, S., Shelley, R., Bowie, A., Perron, M. M. G., and Duce, R. A.: Reviews and syntheses: the GESAMP atmospheric iron deposition model intercomparison study, Biogeosciences, 15, 6659-6684, 10.5194/bg-15-6659-2018, 2018.

Ng, N. L., Herndon, S. C., Trimborn, A., Canagaratna, M. R., Croteau, P. L., Onasch, T. B., Sueper, D., Worsnop, D. R., Zhang, Q., Sun, Y. L., and Jayne, J. T.: An Aerosol Chemical Speciation Monitor (ACSM) for Routine Monitoring of the Composition and Mass Concentrations of Ambient Aerosol, Aerosol. Sci. Tech., 45, 780-794, 10.1080/02786826.2011.560211, 2011.

Peng, X., Xie, T.-T., Tang, M.-X., Cheng, Y., Peng, Y., Wei, F.-H., Cao, L.-M., Yu, K., Du, K., He, L.-Y., and Huang, X.-F.: Critical Role of Secondary Organic Aerosol in Urban

Atmospheric Visibility Improvement Identified by Machine Learning, Environ. Sci. Technol. Lett., 10, 976-982, 10.1021/acs.estlett.3c00084, 2023.

Pöhlker, M. L., Pöhlker, C., Quaas, J., Mülmenstädt, J., Pozzer, A., Andreae, M. O., Artaxo, P., Block, K., Coe, H., Ervens, B., Gallimore, P., Gaston, C. J., Gunthe, S. S., Henning, S., Herrmann, H., Krüger, O. O., McFiggans, G., Poulain, L., Raj, S. S., Reyes-Villegas, E., Royer, H. M., Walter, D., Wang, Y., and Pöschl, U.: Global organic and inorganic aerosol hygroscopicity and its effect on radiative forcing, Nat. Commun., 14, 6139, 10.1038/s41467-023-41695-8, 2023.

Qi, J., Xiong, W., Li, J., Zheng, J., Ye, Q., and Hu, M.: Investigating non-linear and synergistic effects of urban functional zone morphology on land surface temperature, Sustain. Cities Soc., 130, 106546, 10.1016/j.scs.2025.106546, 2025.

Qin, Y., Ye, J., Ohno, P., Liu, P., Wang, J., Fu, P., Zhou, L., Li, Y. J., Martin, S. T., and Chan, C. K.: Assessing the Nonlinear Effect of Atmospheric Variables on Primary and Oxygenated Organic Aerosol Concentration Using Machine Learning, ACS Earth Space Chem., 6, 1059-1066, 10.1021/acsearthspacechem.1c00443, 2022.

Sharma, B., Jia, S., Polana, A. J., Ahmed, M. S., Haque, R. R., Singh, S., Mao, J., and Sarkar, S.: Seasonal variations in aerosol acidity and its driving factors in the eastern Indo-Gangetic Plain: A quantitative analysis, Chemosphere, 305, 135490, 10.1016/j.chemosphere.2022.135490, 2022.

Shi, G., Xu, J., Shi, X., Liu, B., Bi, X., Xiao, Z., Chen, K., Wen, J., Dong, S., Tian, Y., Feng, Y., Yu, H., Song, S., Zhao, Q., Gao, J., and Russell, A. G.: Aerosol pH Dynamics During Haze Periods in an Urban Environment in China: Use of Detailed, Hourly, Speciated Observations to Study the Role of Ammonia Availability and Secondary Aerosol Formation and Urban Environment, J. Geophys. Res.-Atmos., 124, 9730-9742, 10.1029/2018jd029976, 2019.

Song, C., Becagli, S., Beddows, D. C. S., Brean, J., Browse, J., Dai, Q., Dall'Osto, M., Ferracci, V., Harrison, R. M., Harris, N., Li, W., Jones, A. E., Kirchgassner, A., Kramawijaya, A. G., Kurganskiy, A., Lupi, A., Mazzola, M., Severi, M., Traversi, R., and Shi, Z.: Understanding Sources and Drivers of Size-Resolved Aerosol in the High Arctic Islands

of Svalbard Using a Receptor Model Coupled with Machine Learning, Environ. Sci. Technol., 56, 11189-11198, 10.1021/acs.est.1c07796, 2022.

Song, S., Gao, M., Xu, W., Shao, J., Shi, G., Wang, S., Wang, Y., Sun, Y., and McElroy, M. B.: Fine-particle pH for Beijing winter haze as inferred from different thermodynamic equilibrium models, Atmos. Chem. Phys., 18, 7423-7438, 10.5194/acp-18-7423-2018, 2018.

Su, H., Cheng, Y., and Poschl, U.: New Multiphase Chemical Processes Influencing Atmospheric Aerosols, Air Quality, and Climate in the Anthropocene, Acc. Chem. Res., 53, 2034-2043, 10.1021/acs.accounts.0c00246, 2020.

Tao, J., Wu, Y., Deng, Y., Hu, B., and Zhou, Z.: Thermodynamic regulation of aerosol pH by temperature and humidity: The role of gas-particle partitioning of semi-volatile inorganic species in a subtropical region, Environ. Res., 286, 122727, 10.1016/j.envres.2025.122727, 2025.

Tao, Y. and Murphy, J. G.: The Mechanisms Responsible for the Interactions among Oxalate, pH, and Fe Dissolution in PM2.5, ACS Earth Space Chem., 3, 2259-2265, 10.1021/acsearthspacechem.9b00172, 2019.

Tao, Y. and Murphy, J. G.: Simple Framework to Quantify the Contributions from Different Factors Influencing Aerosol pH Based on NH(x) Phase-Partitioning Equilibrium, Environ. Sci. Technol., 55, 10310-10319, 10.1021/acs.est.1c03103, 2021.

Tilgner, A., Schaefer, T., Alexander, B., Barth, M., Collett, J. L., Jr., Fahey, K. M., Nenes, A., Pye, H. O. T., Herrmann, H., and McNeill, V. F.: Acidity and the multiphase chemistry of atmospheric aqueous particles and clouds, Atmos. Chem. Phys., 21, 13483-13536, 10.5194/acp-21-13483-2021, 2021.

Wang, G., Tao, Y., Chen, J., Liu, C., Qin, X., Li, H., Yun, L., Zhang, M., Zheng, H., Gui, H., Liu, J., Huo, J., Fu, Q., Deng, C., and Huang, K.: Quantitative Decomposition of Influencing Factors to Aerosol pH Variation over the Coasts of the South China Sea, East China Sea, and Bohai Sea, Environ. Sci. Technol. Lett., 9, 815-821, 10.1021/acs.estlett.2c00527, 2022.

Wang, G., Zhang, R., Gomez, M. E., Yang, L., Levy Zamora, M., Hu, M., Lin, Y., Peng, J., Guo,

S., Meng, J., Li, J., Cheng, C., Hu, T., Ren, Y., Wang, Y., Gao, J., Cao, J., An, Z., Zhou, W., Li, G., Wang, J., Tian, P., Marrero-Ortiz, W., Secrest, J., Du, Z., Zheng, J., Shang, D., Zeng, L., Shao, M., Wang, W., Huang, Y., Wang, Y., Zhu, Y., Li, Y., Hu, J., Pan, B., Cai, L., Cheng, Y., Ji, Y., Zhang, F., Rosenfeld, D., Liss, P. S., Duce, R. A., Kolb, C. E., and Molina, M. J.: Persistent sulfate formation from London Fog to Chinese haze, Proc Natl Acad Sci U S A, 113, 13630-13635, 10.1073/pnas.1616540113, 2016.

Wang, J., Wu, Z., Qiu, T., Man, R., Zong, T., Qiu, Y., Fang, W., Chen, S., Liang, D., Song, M., Ahn, J., Lee, J., and Hu, M.: Impacts of aerosol acidity and liquid water content on secondary inorganic aerosol pollution in East Asian megacities: Beijing and Seoul, Atmos. Environ., 361, 10.1016/j.atmosenv.2025.121479, 2025.

Wang, S., Wang, L., Li, Y., Wang, C., Wang, W., Yin, S., and Zhang, R.: Effect of ammonia on fine-particle pH in agricultural regions of China: comparison between urban and rural sites, Atmos. Chem. Phys., 20, 2719-2734, 10.5194/acp-20-2719-2020, 2020.

Wang, Y. C., Huang, R. J., Ni, H. Y., Chen, Y., Wang, Q. Y., Li, G. H., Tie, X. X., Shen, Z. X., Huang, Y., Liu, S. X., Dong, W. M., Xue, P., Fröhlich, R., Canonaco, F., Elser, M., Daellenbach, K. R., Bozzetti, C., El Haddad, I., Prévôt, A. S. H., Canagaratna, M. R., Worsnop, D. R., and Cao, J. J.: Chemical composition, sources and secondary processes of aerosols in Baoji city of northwest China, Atmos. Environ., 158, 128-137, 10.1016/j.atmosenv.2017.03.026, 2017.

Wei, N., Jia, Z., Men, Z., Ren, C., Zhang, Y., Peng, J., Wu, L., Wang, T., Zhang, Q., and Mao, H.: Machine Learning Predicts Emissions of Brake Wear PM2.5: Model Construction and Interpretation, Environ. Sci. Technol. Lett., 9, 352-358, 10.1021/acs.estlett.2c00117, 2022.

Wei, Y., Wang, S., Jiang, N., Zhang, R., and Hao, Q.: Comparative multi-model study of PM(2.5) acidity trend changes in ammonia-rich regions in winter: Based on a new ammonia concentration assessment method, J. Hazard. Mater., 458, 131970, 10.1016/j.jhazmat.2023.131970, 2023.

Xie, F., Su, Y., Tian, Y., Shi, Y., Zhou, X., Wang, P., Yu, R., Wang, W., He, J., Xin, J., and Lü, C.: The shifting of secondary inorganic aerosol formation mechanisms during haze aggravation: the decisive role of aerosol liquid water, Atmos. Chem. Phys., 23, 2365-2378,

637 10.5194/acp-23-2365-2023, 2023.
638 Xie, Y., Wang, G., Wang, X., Chen, J., Chen, Y., Tang, G., Wang, L., Ge, S., Xue, G., Wang, Y.,
639 and Gao, J.: Nitrate-dominated PM2.5 and elevation of particle pH observed in urban
640 Beijing during the winter of 2017, Atmos. Chem. Phys., 20, 5019-5033, 10.5194/acp-20-
641 5019-2020, 2020.
642 Xu, K., Yin, L., Chen, Q., Liao, D., Ji, X., Zhang, K., Wu, Y., Xu, L., Li, M., Fan, X., Zhang,
643 F., Huang, Z., Chen, J., and Hong, Y.: Quantitative analysis of influencing factors to
644 aerosol pH and its responses to PM(2.5) and O(3) pollution in a coastal city, J. Environ.
645 Sci., 151, 284-297, 10.1016/j.jes.2024.03.044, 2025.
646 Yang, C., Dong, H., Chen, Y., Wang, Y., Fan, X., Tham, Y. J., Chen, G., Xu, L., Lin, Z., Li, M.,
647 Hong, Y., and Chen, J.: Machine Learning Reveals the Parameters Affecting the Gaseous
648 Sulfuric Acid Distribution in a Coastal City: Model Construction and Interpretation,
649 Environ. Sci. Technol. Lett., 10, 1045-1051, 10.1021/acs.estlett.3c00170, 2023.
650 Yang, C., Dong, H., Chen, Y., Xu, L., Chen, G., Fan, X., Wang, Y., Tham, Y. J., Lin, Z., Li, M.,
651 Hong, Y., and Chen, J.: New Insights on the Formation of Nucleation Mode Particles in a
652 Coastal City Based on a Machine Learning Approach, Environ. Sci. Technol., 58, 1187-
653 1198, 10.1021/acs.est.3c07042, 2024.
654 Yang, J., Wang, S., Zhang, R., and Yin, S.: Elevated particle acidity enhanced the sulfate
655 formation during the COVID-19 pandemic in Zhengzhou, China, Environ. Pollut., 296,
656 118716, 10.1016/j.envpol.2021.118716, 2022.
657 Zhang, B., Shen, H., Liu, P., Guo, H., Hu, Y., Chen, Y., Xie, S., Xi, Z., Skipper, T. N., and
658 Russell, A. G.: Significant contrasts in aerosol acidity between China and the United States,
659 Atmos. Chem. Phys., 21, 8341-8356, 10.5194/acp-21-8341-2021, 2021.
660 Zheng, G., Su, H., Wang, S., Andreae, M. O., Pöschl, U., and Cheng, Y.: Multiphase buffer
661 theory explains contrasts in atmospheric aerosol acidity, Science, 369, 1374-1377, 2020.
662 Zhou, M., Zheng, G., Wang, H., Qiao, L., Zhu, S., Huang, D., An, J., Lou, S., Tao, S., Wang,
663 Q., Yan, R., Ma, Y., Chen, C., Cheng, Y., Su, H., and Huang, C.: Long-term trends and
664 drivers of aerosol pH in eastern China, Atmos. Chem. Phys., 22, 13833-13844,
665 10.5194/acp-22-13833-2022, 2022.

Supporting information for

Quantitative insights into regime-dependent aerosol pH variability in ~~an~~ ammonia-rich urban Beijing ~~atmosphere~~ from explainable machine learning

Jing Duan[1,†], Ting Wang[1,†], Ru-Jin Huang[1,2,3*], Jingye Ren[1], Haobin Zhong[4], Wei Xu[5], Chunshui Lin[1], Yanan Zhan[1,2], Huabin Huang[6], Yongjie Li[7]

[1]State Key Laboratory of Loess Science, Institute of Earth Environment, Chinese Academy of Sciences, Xi'an 710061, China

[2]Institute of Global Environmental Change, Xi'an Jiaotong University, Xi'an 710049, China

[3]University of Chinese Academy of Sciences, Beijing 100049, China

[4]School of Advanced Materials Engineering, Jiaxing Nanhu University, Jiaxing, 314001, China

[5]State Key Laboratory of Advanced Environmental Technology, Institute of Urban Environment, Chinese Academy of Sciences, Xiamen, China

[6]College of Environment and Public Health, Xiamen Huaxia University, Xiamen 361024, China

[7]Department of Civil and Environmental Engineering, Faculty of Science and Technology, University of Macau, Taipa, Macau SAR 999078, China

Correspondence to: Ru-Jin Huang (rujin.huang@ieecas.cn)

†Contributed equally to this study

Text S1. Sampling and instrumentation

The field campaign was carried out at an urban site located on the rooftop of a five-story building (~20 m above ground) at the National Center for Nanoscience in Beijing (39.99°N, 116.32°E). The site is situated near the 4th Ring Road and is influenced by mixed residential, commercial, and traffic emissions (Duan et al., 2020; Gu et al., 2020). Continuous measurements were performed from 21 December 2014 to 31 December 2015.

Non-refractory PM_1 (NR-PM_1) species, including organics (OA), sulfate (SO_4^{2-}), nitrate (NO_3^-), ammonium (NH_4^+), and chloride (Cl^-), were quantified using an Aerodyne quadrupole aerosol chemical speciation monitor (Q-ACSM) with a time resolution of ~30 min (Ng et al., 2011). Ambient aerosols were sampled through a 3/8 in. stainless-steel tube at a flow rate of ~ 3 L min^{-1}, and the coarse particles were removed by an University Research Glassware (URG) cyclone (model: URG2000-30ED) with a 2.5 μm cut in front of the sampling inlet. Before entering the ACSM, particles were dried using a Nafion dryer (MD110-48S; Perma Pure, Inc., Lakewood, NJ, USA). The dried submicron aerosol was then subsampled into the ACSM at 85 cc min^{-1}, controlled by a 100 μm critical orifice. Within the ACSM, particles were focused into a narrow beam by an aerodynamic lens and vaporized on a heated surface (~600 °C). The resulting vapor was ionized with electron impact and chemically characterized with a quadrupole mass spectrometer. Instrument calibration was carried out using monodisperse 300 nm ammonium nitrate particles generated by an atomizer (Model 9302, TSI Inc., Shoreview, MN, USA) and size-selected by a differential mobility analyzer (DMA; TSI Model 3080) to determine the response factor (RF) and ionization efficiency (IE) (Ng et al., 2011).

Ambient ammonia (NH_3) concentrations were measured using a Picarro G2103 analyzer (Picarro Inc., USA), which employs wavelength-scanning optical cavity ring down spectroscopy (WS-CRDS). This technique is capable of measuring NH_3 with a parts-per-trillion (ppt) sensitivity based on a sophisticated time-based measurement system (Maasikmets et al., 2015). The G2103 is equipped with high-precision temperature and pressure control systems to ensure the highest accuracy and lowest drift. In addition, the G2103 offers a large dynamic range, providing linear response into the parts-per-million (ppm) range without dilution,

concentration and sample preparation.

Meteorological parameters, including temperature and relative humidity (RH), were simultaneously recorded by an automatic weather station (MAWS201, Vaisala, Vantaa, Finland).

Text S2. Calculation of excess NHx

Excess NHx in this study represents the portion of total NHx (gas-phase NH_3 plus particle-phase NH_4^+) that remains after neutralizing the major inorganic acidic species (SO_4^{2-}, NO_3^-, and Cl^-) in the aerosol (i.e., the required NHx) (Liu et al., 2017).

Thus, excess NHx is defined as:

Excess NHx = Total NHx- Requid NHx

Where

$$\text{Total NHx} = 17 \times \left(\frac{[NH_3]}{17} + \frac{[NH_4^+]}{18}\right) \quad (1)$$

$$\text{Required NHx} = 17 \times \left(\frac{[SO_4^{2-}]}{48} + \frac{[NO_3^-]}{62} + \frac{[Cl^-]}{35.5}\right) \quad (2)$$

$[NH_3]$, $[NH_4^+]$, $[SO_4^{2-}]$, $[NO_3^-]$, and $[Cl^-]$ are the measured mass concentrations (μg m^{-3}). A positive excess NHx (μg m^{-3}) indicates ammonia-rich conditions, whereas a negative value denotes ammonia-poor conditions (Song et al., 2018).

Table S1. Monthly performance metrics (R^2, RMSE, MAE) of the XGBoost model from leave-one-month-out cross-validation.

Month	R^2	RMSE	MAE
Dec-14	0.64	0.23	0.15
Jan-15	0.63	0.19	0.16
Feb-15	0.68	0.23	0.17
Mar-15	0.90	0.21	0.15
Apr-15	0.94	0.17	0.12
May-15	0.97	0.13	0.08
Jun-15	0.98	0.10	0.07
Jul-15	0.97	0.10	0.06

Aug-15	0.96	0.13	0.10
Sep-15	0.94	0.19	0.11
Oct-15	0.88	0.19	0.12
Nov-15	0.90	0.11	0.08
Dec-15	0.74	0.19	0.15
Average	**0.86±0.13**	**0.17±0.05**	**0.12±0.04**

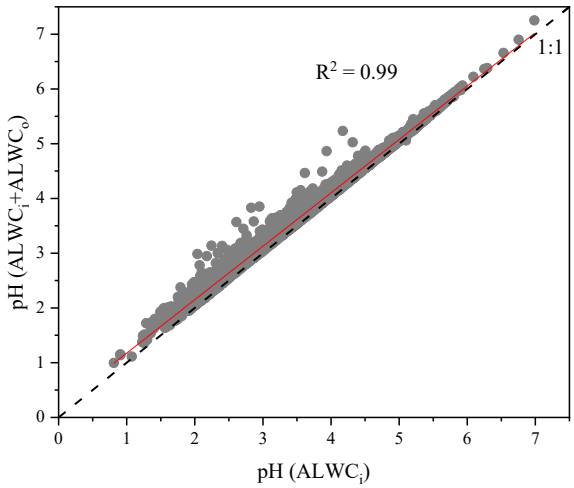

Figure S1. Comparison of pH calculated with and without organic aerosol water (ALWC$_o$).

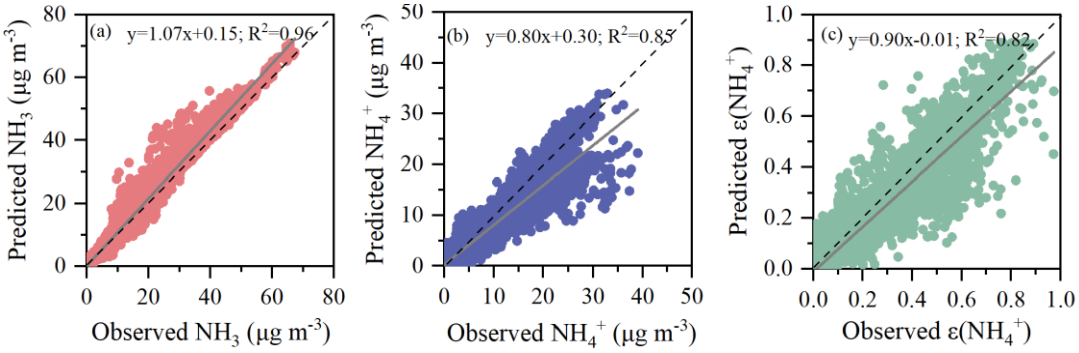

Figure ~~S1~~S2. Comparisons between predicted and observed values for NH_3 (a), NH_4^+ (b), and $\varepsilon(NH_4^+)$ (c). $\varepsilon(NH_4^+)$ is calculated as the molar ratio of $NH_4^+/(NH_4^+ + NH_3)$.

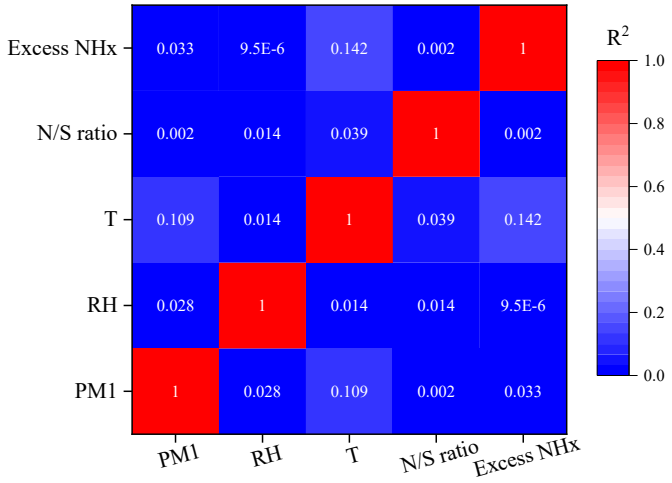

Figure S3. Correlation matrix of input features. The color scale represents the correlation coefficient (R^2).

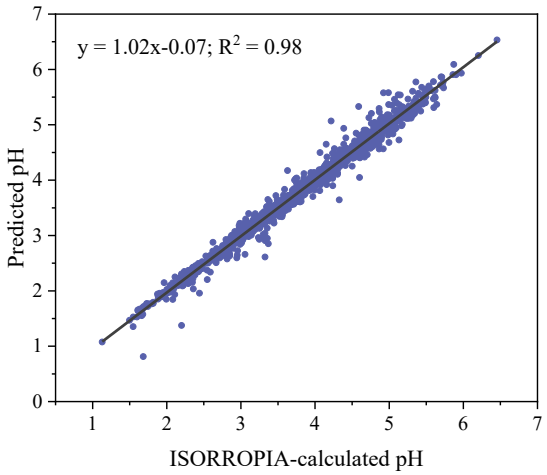

Figure ~~S2~~S4. Correlation between aerosol pH predicted by XGBoost model and pH calculated using ISORRPOIA II.

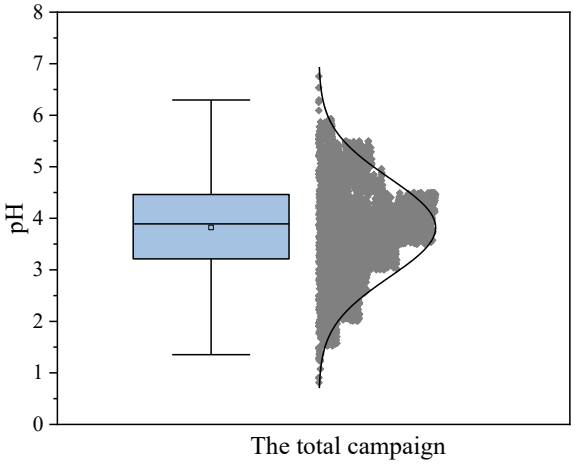

Figure S5. Distribution of aerosol pH in this study. The box spans the 25th–75th percentiles, with whiskers extending to the 10th and 90th percentiles. The line and square inside the box indicate the median and mean, respectively.

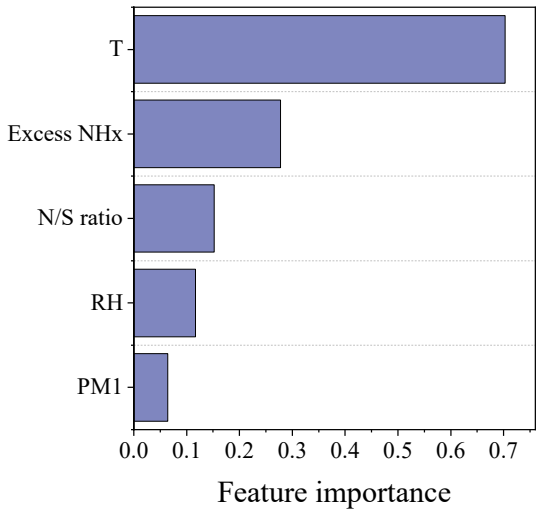

Figure ~~S3~~S6. Feature importance for aerosol pH over the entire sampling period based on mean absolute SHAP values.

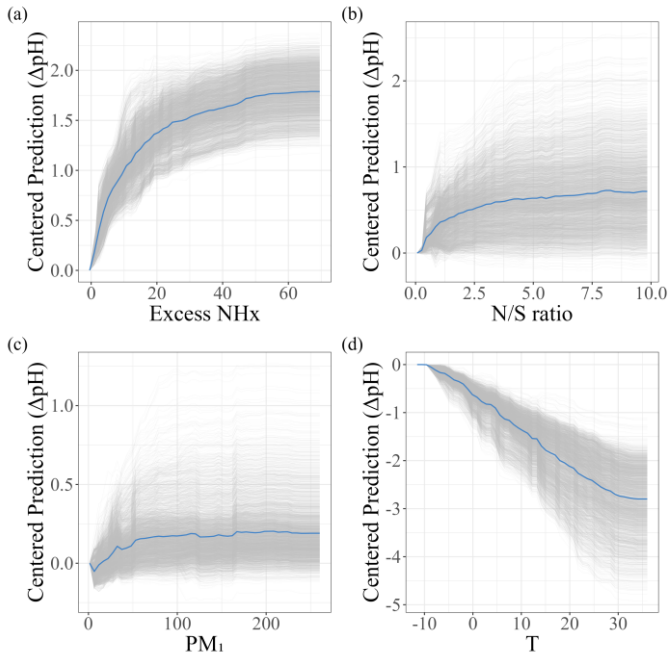

Figure S7. c-ICE curves of (a) Excess NHx (μg m^{-3}), (b) N/S ratio, (c) PM_1 mass loading (μg m^{-3}), and (d) temperature (T, ℃). Gray lines represent sample-specific effects on aerosol pH, and the blue line shows the averaged response.

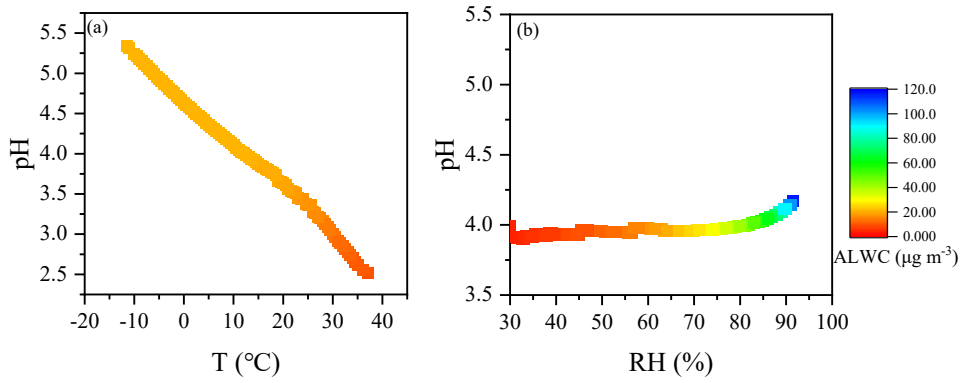

Figure ~~S4~~S8. ISORROPIA II sensitivity tests of pH to temperature (a) and RH (b). In this analysis, the real-time measured values of the tested variable, while the average values of the other species were applied as the input into ISORROPIA II.

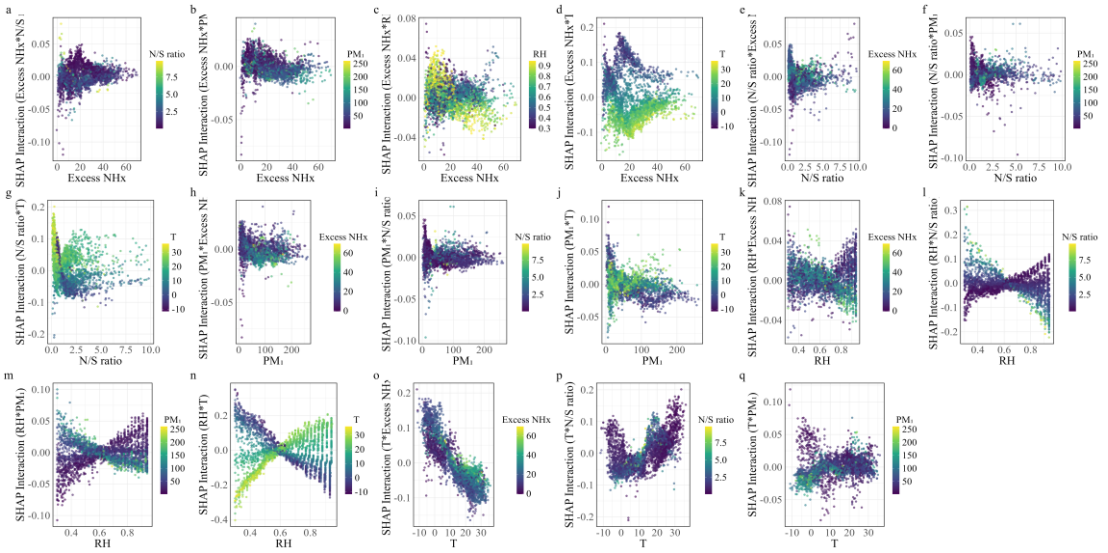

Figure ~~S5~~S9. Summary plots of the SHAP interaction matrix values for pH among each pair of variables, excluding RH vs T, RH vs N/S ratio, and RH vs PM_1 mass, which are discussed in detail in the manuscript.

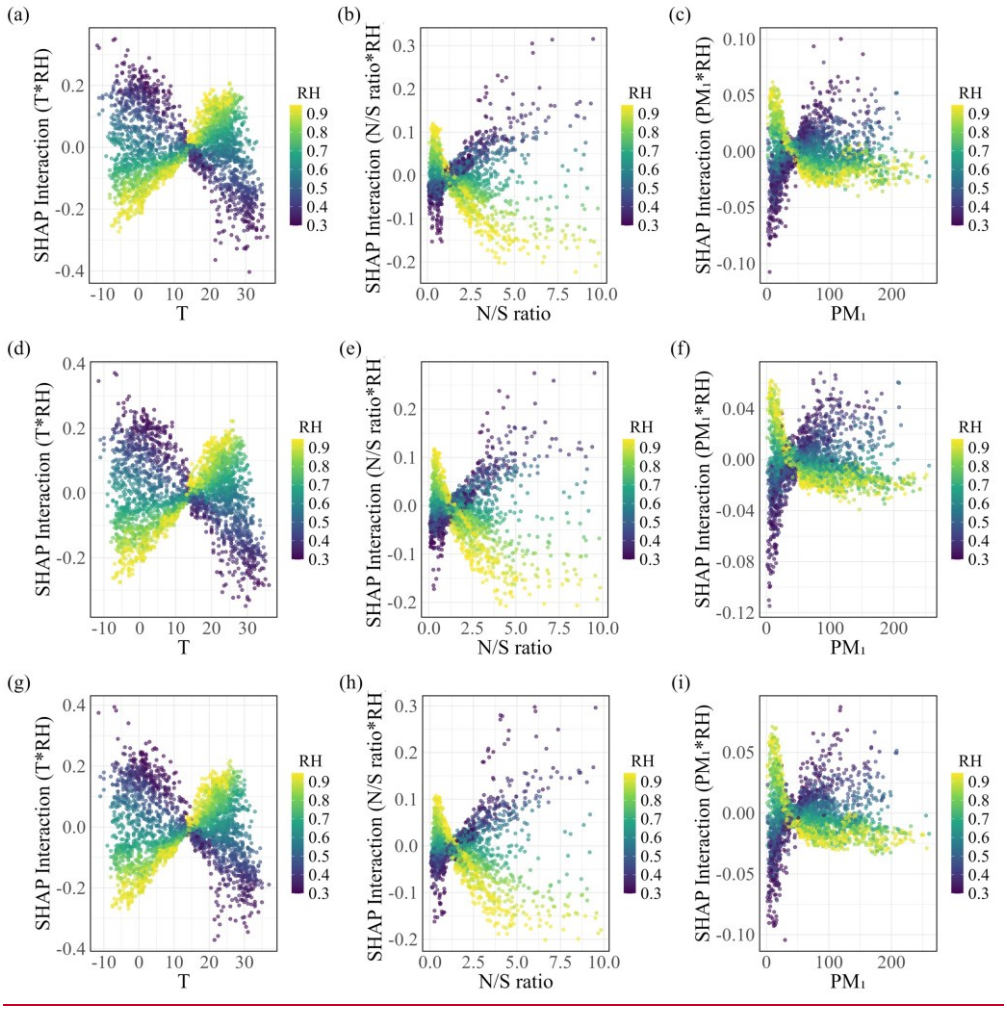

Figure S10. SHAP interaction plots for RH versus temperature (T, °C), N/S ratio, and PM_1 mass loading (μg m^{-3}) under different random seeds of 1234 (a, b, c), 5678 (d, e, f), and 9012 (g, h, i). The color scale represents RH, and the SHAP interaction values indicate the direction and magnitude of the interactive contributions to pH across different regimes.

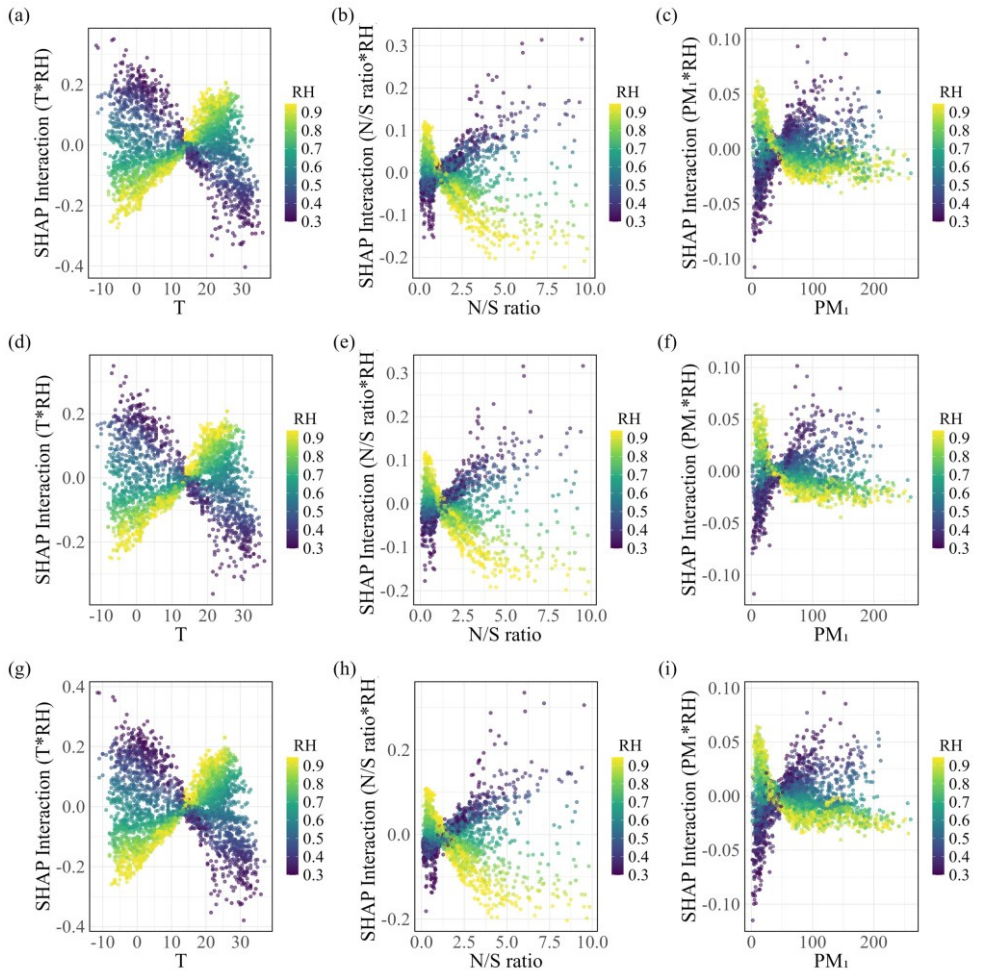

Figure S11. SHAP interaction plots for RH versus temperature (T, °C), N/S ratio, and PM_1 mass loading (μg m^{-3}) under different train/test split ratio of 0.7 (a, b, c), 0.6 (d, e, f), and 0.8 (g, h, i). The color scale represents RH, and the SHAP interaction values indicate the direction and magnitude of the interactive contributions to pH across different regimes.

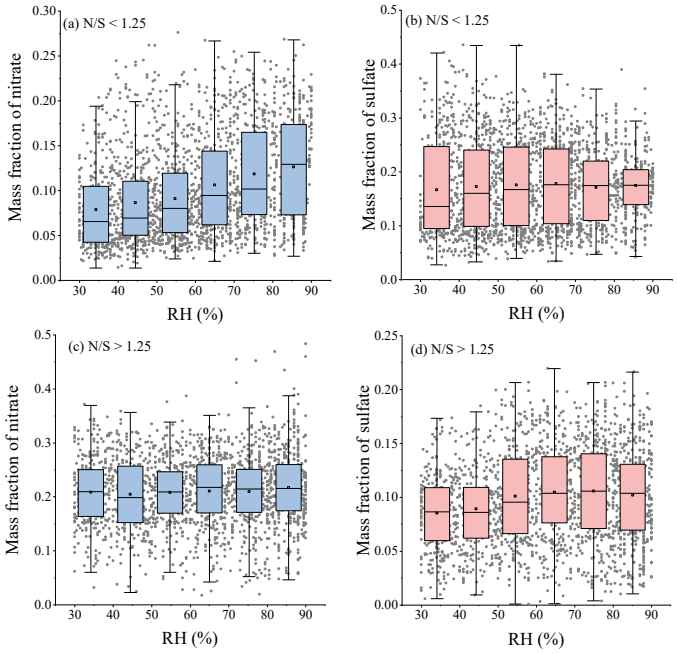

Figure ~~S6~~S12. The variations in nitrate and sulfate mass fractions with RH under sulfate-dominant conditions (N/S < 1.25) (a, b) and nitrate-dominant conditions (N/S > 1.25) (c, d), respectively. The whiskers, floating boxes, lines, and squares inside the boxes denote the 10th and 90th distributions, 25th-75th ranges, median values, and mean values, respectively.

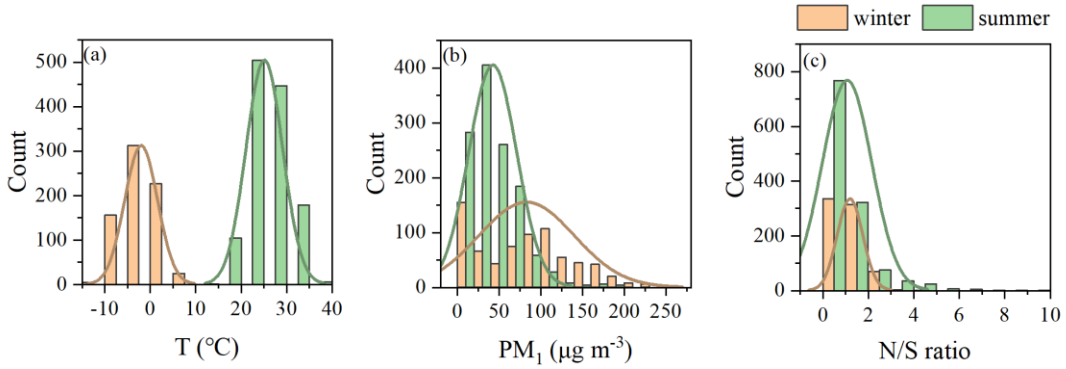

Figure ~~S7~~S13. The distribution of temperature (a), PM_1 mass loading (b), and nitrate-to-sulfate (N/S) mass ratio (c) between summer and winter periods.

Reference

Duan, J., Huang, R.-J., Li, Y., Chen, Q., Zheng, Y., Chen, Y., Lin, C., Ni, H., Wang, M., Ovadnevaite, J., Ceburnis, D., Chen, C., Worsnop, D. R., Hoffmann, T., O'Dowd, C., and

Cao, J.: Summertime and wintertime atmospheric processes of secondary aerosol in Beijing, Atmos. Chem. Phys., 20, 3793-3807, 10.5194/acp-20-3793-2020, 2020.

Gu, Y., Huang, R. J., Li, Y., Duan, J., Chen, Q., Hu, W., Zheng, Y., Lin, C., Ni, H., Dai, W., Cao, J., Liu, Q., Chen, Y., Chen, C., Ovadnevaite, J., Ceburnis, D., and O'Dowd, C.: Chemical nature and sources of fine particles in urban Beijing: Seasonality and formation mechanisms, Environ. Int., 140, 105732, 10.1016/j.envint.2020.105732, 2020.

Liu, M., Song, Y., Zhou, T., Xu, Z., Yan, C., Zheng, M., Wu, Z., Hu, M., Wu, Y., and Zhu, T.: Fine particle pH during severe haze episodes in northern China, Geophys. Res. Lett., 44, 5213-5221, 10.1002/2017gl073210, 2017.

Maasikmets, M., Teinemaa, E., Kaasik, A., and Kimmel, V.: Measurement and analysis of ammonia, hydrogen sulphide and odour emissions from the cattle farming in Estonia, Biosyst. Eng., 139, 48-59, 10.1016/j.biosystemseng.2015.08.002, 2015.

Ng, N. L., Herndon, S. C., Trimborn, A., Canagaratna, M. R., Croteau, P. L., Onasch, T. B., Sueper, D., Worsnop, D. R., Zhang, Q., Sun, Y. L., and Jayne, J. T.: An Aerosol Chemical Speciation Monitor (ACSM) for Routine Monitoring of the Composition and Mass Concentrations of Ambient Aerosol, Aerosol. Sci. Tech., 45, 780-794, 10.1080/02786826.2011.560211, 2011.

Song, S., Gao, M., Xu, W., Shao, J., Shi, G., Wang, S., Wang, Y., Sun, Y., and McElroy, M. B.: Fine-particle pH for Beijing winter haze as inferred from different thermodynamic equilibrium models, Atmos. Chem. Phys., 18, 7423-7438, 10.5194/acp-18-7423-2018, 2018.